Nodal Galerkin Methods for Numerical Modelling of Linear Elasticity

Matthew A. McDonald*, Michael P. Lamoureux and Gary F. Margrave

ABSTRACT

We consider here a method for numerical propagation of elastic waves in heterogeneous media based on the weak formulation of the elastodynamic equilibrium equations. The method provides high accuracy in the spatial domain and converges exponentially. It is appropriate for any formulation of the elastic wave equation in any number of spatial dimensions, but for simplicity is only presented here for isotropic media. Absorbing boundary conditions are incorporated into the method naturally and various time-stepping algorithms are investigated. In the conclusion we compare various implementations of the method to second and fourth order finite differences.

INTRODUCTION

This report is split up into four sections, each with its own purpose. The first section is on the weak formulation of the elastic wave equation and the analysis that goes along with redefining the problem. This is all fairly tedious and mathematically involved, but must be done once in order to derive a numerical method as well as to ensure solutions to the new problem are meaningful. One could safely skip this section by taking note of the newly formulated problem in equations (4) and (6).

The second section derives the nodal Galerkin numerical method for the new problem. The intent of this section is to write down the stumbling blocks that were encountered when building the numerical schemes and present them in a way that may be more accessible. Once the numerical scheme is constructed some comparisons of the method with second and fourth order finite-differences are made.

Lastly, an appendix presents all of the background material and construction of some of the aspects of the method that are not entirely required to understand the broader picture.

WEAK FORMULATION OF THE ELASTIC WAVE EQUATION

Consider the *strong* formulation of the elastic wave equation for an arbitrary isotropic heterogeneous medium $\Omega \in \mathbb{R}^d, d = 1, 2, 3$, with boundary $\partial\Omega := \Gamma$.

$$\text{Find } \boldsymbol{u} \in C^2(\Omega), \text{such that} \begin{cases} \rho\ddot{u}_i = \partial_j \sigma_{ij}(\boldsymbol{u}) + f_i. \\ \boldsymbol{u}(\boldsymbol{x}, t = 0) = \boldsymbol{u}_0(\boldsymbol{x}) \ , \forall \boldsymbol{x} \in \Omega, t >= 0 \\ \dot{\boldsymbol{u}}(\boldsymbol{x}, t = 0) = \boldsymbol{u}_1(\boldsymbol{x}) \end{cases} \tag{1}$$

The stress and strain tensors are related by

$$\sigma_{ij}(\boldsymbol{u}) = \lambda(\nabla \cdot \boldsymbol{u})\delta_{ij} + 2\mu\varepsilon_{ij}(\boldsymbol{u})$$

where ∂_j denotes differentiation with respect to the j^{th} element x_j. Summation over repeated indices, as per Einstein notation, is assumed unless otherwise noted. The parameters λ, μ and ρ are the elastic constants of the medium and all may be bounded, spatially dependent, functions. $f_i(\boldsymbol{x}, t)$ is the i^{th} component of the body force applied to the medium.

We obtain the *weak* form of the dynamic equilibrium equations through a standard *Galerkin* weighted-residuals approach. Omitting the rigorous mathematical details for the moment we multiply both sides of (1) by an arbitrary test function $v \equiv v(\boldsymbol{x})$ and integrate over the entire space. This yields

$$\int_\Omega \rho \ddot{u}_i v d\Omega = \int_\Omega \partial_j \sigma_{ij}(\boldsymbol{u}) v d\Omega + \int_\Omega f_i v d\Omega. \tag{2}$$

Expanding the first term on the right hand side and applying Green's theorem yields the relationship

$$\int_\Omega \partial_j \sigma_{ij}(\boldsymbol{u}) v d\Omega = \oint_\Gamma \sigma_{ij}(\boldsymbol{u}) v \hat{n}_j d\Gamma - \int_\Omega \sigma_{ij}(\boldsymbol{u}) \partial_j v d\Omega.$$

where $\hat{n}_j$ denotes the direction cosine between the outward-pointing normal vector and the j^{th} elementary basis vector. Substituting this into (2) yields the weak variational form of (1)

$$\int_\Omega \rho \ddot{u}_i v d\Omega + \int_\Omega \sigma_{ij}(\boldsymbol{u}) \partial_j v d\Omega = \int_\Omega f_i v d\Omega + \oint_\Gamma \sigma_{ij}(\boldsymbol{u}) v \hat{n}_j d\Gamma. \tag{3}$$

This is the form for the i^{th} component of displacement, $i = 1, \ldots, d$. Introducing the arbitrary vector-valued function $\boldsymbol{v} \equiv \boldsymbol{v}(\boldsymbol{x})$, with arbitrary components, we may then add the d equations together to obtain

$$\frac{d^2}{dt^2} \int \rho \boldsymbol{u} \cdot \boldsymbol{v} d\Omega + \int_\Omega \sigma_{ij}(\boldsymbol{u}) \partial_j v_i d\Omega = \int_\Omega \boldsymbol{f} \cdot \boldsymbol{v} d\Omega + \oint_\Gamma \sigma_{ij}(\boldsymbol{u}) \hat{n}_j v_i d\Gamma. \tag{4}$$

For simplicity we present the following derivation for $d = 2$, but the result is the same in any number of dimensions. Expanding the integrand of the second term on the left hand side of (4) produces

$$\begin{aligned} &\sigma_{11}(\boldsymbol{u}) \partial_1 v_1 + \sigma_{12}(\boldsymbol{u}) \partial_2 v_1 + \sigma_{21}(\boldsymbol{u}) \partial_1 v_2 + \sigma_{22}(\boldsymbol{u}) \partial_2 v_2 \\ &= \sigma_{11}(\boldsymbol{u}) \varepsilon_{11}(\boldsymbol{v}) + \sigma_{12}(\boldsymbol{u}) \partial_2 v_1 + \sigma_{21}(\boldsymbol{u}) \partial_1 v_2 + \sigma_{22}(\boldsymbol{u}) \varepsilon_{22}(\boldsymbol{v}) \end{aligned} \tag{5}$$

adding together the second and third terms in (5) yields

$$\begin{aligned} &\mu(\partial_1 u_2 + \partial_2 u_1) \partial_2 v_1 + \mu(\partial_2 u_1 + \partial_1 u_2) \partial_1 v_2 \\ &= \mu(\partial_1 u_2 + \partial_2 u_1)(\partial_2 v_1 + \partial_1 v_2) \\ &= \sigma_{12}(\boldsymbol{u}) \varepsilon_{12}(\boldsymbol{v}) + \sigma_{21}(\boldsymbol{u}) \varepsilon_{21}(\boldsymbol{v}). \end{aligned}$$

So we obtain

$$\int_\Omega \sigma_{ij}(\boldsymbol{u}) \partial_j v_i d\Omega = \int_\Omega \sigma_{ij}(\boldsymbol{u}) \varepsilon_{ij}(\boldsymbol{v}) d\Omega$$

If we then define the vector $\boldsymbol{T}$ component-wise by

$$T_i = \sigma_{ij}(\boldsymbol{u}) \hat{n}_j$$

we may write the second term in the right hand side of (4) as

$$\int_\Gamma \sigma_{ij}(\boldsymbol{u}) \hat{n}_j v_i d\Gamma = \oint_\Gamma \boldsymbol{T} \cdot \boldsymbol{v} d\Gamma$$

and so (3) becomes

$$\frac{d^2}{dt^2}\int \rho \boldsymbol{u}\cdot\boldsymbol{v}d\Omega + \int_\Omega \sigma_{ij}(\boldsymbol{u})\varepsilon_{ij}(\boldsymbol{v})d\Omega = \int_\Omega \boldsymbol{f}\cdot\boldsymbol{v}d\Omega + \oint_\Gamma \boldsymbol{T}\cdot\boldsymbol{v}d\Gamma i,j=1,\ldots,d.$$

Further discussion, including derivation for a full elastic tensor, as well as a proof of the equivalence of the weighted-residuals approach with the principal of virtual work, can be found in chapter three of (Zienkiewicz et al., 2005).

In order to make the variational approach rigorous we need to identify a few function spaces in which our various trial and test function will reside. Define $H^1(\Omega)$ to be the classic Sobolev space of square integrable functions defined on Ω, with square-integrable weak first derivatives. That is,

$$H^1(\Omega) = \left\{ f \in L^2(\Omega) | D^1 f \in L^2(\Omega) \right\},$$

where

$$L^2(\Omega) = \left\{ f : \Omega \to \mathbb{R} | \int_\Omega |f(\boldsymbol{x})|^2 d\Omega < \infty \right\}$$

and D^1 denotes the weak first derivative operator.

Then the vector-valued version is defined as those vector-valued functions whose components reside in $H^1(\Omega)$. Denote $L^2(\Omega)^d = L^2(\Omega)\times\cdots\times L^2(\Omega)$ and define this space to be

$$\mathcal{H} = \left\{ \boldsymbol{u}(\boldsymbol{x}) \in L^2(\Omega)^d | \nabla\boldsymbol{u} \in L^2(\Omega)^d \right\}.$$

The variational problem is thus: find $\boldsymbol{u}\in\mathcal{H}$ such that, for all $t\geq 0$,

$$\langle \rho\ddot{\boldsymbol{u}}, \boldsymbol{v}\rangle_\Omega + a(\boldsymbol{u},\boldsymbol{v}) = \langle \boldsymbol{f},\boldsymbol{v}\rangle_\Omega + \langle \boldsymbol{T},\boldsymbol{v}\rangle_\Gamma, \forall \boldsymbol{v}\in\mathcal{H}. \tag{6}$$

The inner-products in (6) are the standard vector-valued $L^2(\Omega)$ inner-products

$$\langle \boldsymbol{u},\boldsymbol{v}\rangle_\Omega = \int_\Omega \boldsymbol{f}\cdot\boldsymbol{g}d\Omega,$$

$$\langle \boldsymbol{u},\boldsymbol{v}\rangle_\Gamma = \oint_\Gamma \boldsymbol{f}\cdot\boldsymbol{g}d\Gamma$$

and the norm on $\mathcal{H}$ is given by

$$\|\boldsymbol{v}\|_{\mathcal{H}} = \left(|\langle \boldsymbol{v},\boldsymbol{v}\rangle_\Omega|^2 + |\langle \nabla\boldsymbol{v},\nabla\boldsymbol{v}\rangle_\Omega|^2 \right)^{1/2}$$

To show that there exists a unique solution to (6) we need to show that

$$a(\boldsymbol{u},\boldsymbol{v}) = \int_\Omega \sigma_{ij}(\boldsymbol{u})\varepsilon_{ij}(\boldsymbol{v})d\Omega$$

is a symmetric, V-elliptic and continuous bi-linear form and apply the Lax-Milgram lemma (Atkinson and Han, 2009).

To see that $a(\boldsymbol{u},\boldsymbol{v})$ is symmetric and bi-linear we must show that the following all hold:

1. $a(\boldsymbol{u}, \boldsymbol{v}) = a(\boldsymbol{v}, \boldsymbol{u}), \forall \boldsymbol{u}, \boldsymbol{v} \in \mathcal{H}$,
2. $a(\boldsymbol{u} + \boldsymbol{u}', \boldsymbol{v}) = a(\boldsymbol{u}, \boldsymbol{v}) + a(\boldsymbol{u}', \boldsymbol{v}), \forall \boldsymbol{u}, \boldsymbol{u}', \boldsymbol{v} \in \mathcal{H}$,
3. $a(\lambda \boldsymbol{u}, \boldsymbol{v}) = \lambda a(\boldsymbol{u}, \boldsymbol{v}), \forall \boldsymbol{u}, \boldsymbol{v} \in \mathcal{H}$, and $\lambda \in \mathbb{R}$.

The second and third equalities follow trivially from the linearly of the derivative. For brevity we show the first equality only for $d = 2$. This follows from expanding $\sigma_{ij}(\boldsymbol{u})\varepsilon_{ij}(\boldsymbol{v})$ as

$$\sigma_{ij}(\boldsymbol{u})\varepsilon_{ij}(\boldsymbol{v}) = \sigma_{11}(\boldsymbol{u})\varepsilon_{11}(\boldsymbol{v}) + \sigma_{12}(\boldsymbol{u})\varepsilon_{12}(\boldsymbol{v}) + \sigma_{21}(\boldsymbol{u})\varepsilon_{21}(\boldsymbol{v}) + \sigma_{22}(\boldsymbol{u})\varepsilon_{22}(\boldsymbol{v}).$$

$$= [\lambda(\nabla\cdot\boldsymbol{u})+2\mu\varepsilon_{11}(\boldsymbol{v})]\varepsilon_{11}(\boldsymbol{v})+2\mu\varepsilon_{12}(\boldsymbol{u})\varepsilon_{12}(\boldsymbol{v})+2\mu\varepsilon_{21}(\boldsymbol{u})\varepsilon_{21}(\boldsymbol{v})+[\lambda(\nabla\cdot\boldsymbol{u})+2\mu\varepsilon_{22}(\boldsymbol{v})]\varepsilon_{22}(\boldsymbol{v}).$$

The terms corresponding to $i \neq j$ are symmetric and so we only need to show that the sum of the $i = j$ terms are as well. Adding together the first and last term produces

$$[\lambda(\nabla \cdot \boldsymbol{u}) + 2\mu\varepsilon_{11}(\boldsymbol{v})]\varepsilon_{11}(\boldsymbol{v}) + [\lambda(\nabla \cdot \boldsymbol{u}) + 2\mu\varepsilon_{22}(\boldsymbol{v})]\varepsilon_{22}(\boldsymbol{v})$$

$$= \lambda(\nabla \cdot \boldsymbol{u})[\varepsilon_{11}(\boldsymbol{v}) + \varepsilon_{22}(\boldsymbol{v})] + 2\mu[\varepsilon_{11}(\boldsymbol{u})\varepsilon_{11}(\boldsymbol{v}) + \varepsilon_{22}(\boldsymbol{u})\varepsilon_{22}(\boldsymbol{v})]$$

$$= \lambda(\nabla \cdot \boldsymbol{u})(\nabla \cdot \boldsymbol{v}) + 2\mu(\nabla\boldsymbol{u} \cdot \nabla\boldsymbol{v})$$

which is symmetric and, thus, $a(\boldsymbol{u}, \boldsymbol{v})$ is symmetric and bi-linear. Continuity follows directly from our assumptions that all the functions included in our scheme are bounded.

A bi-linear form $a(\cdot, \cdot)$ is V-elliptic, or strongly positive, if there exists $C > 0$ such that

$$a(\boldsymbol{v}, \boldsymbol{v}) \geq C\|\boldsymbol{v}\|^2_{\mathcal{H}}, \forall v \in V.$$

This follows directly from Korn's inequality (Horgan, 1995) which ensures us that there exists a constant K depending only on Ω such that:

$$\|\boldsymbol{v}\|^2_{\mathcal{H}} \leq K(\Omega) \int_\Omega \{\boldsymbol{v} \cdot \boldsymbol{v} + \varepsilon_{ij}(\boldsymbol{v})\varepsilon_{ij}(\boldsymbol{v})\}\, d\Omega, \forall \boldsymbol{v} \in \mathcal{H}.$$

CONSTRUCTION OF THE NUMERICAL SCHEMES

The weak formulation of the elastic wave equation provides the basis for a number of numerical methods, ranging from classic methods such as the finite elements and finite volumes, to more obscure methods such as boundary elements, discontinuous Galerkin, and moving least squares. Here we restrict to global methods which seek to approximate the solution to the weak variational problem by decomposing it into a basis of polynomials in space and unknown functions in time. This reduces the problem to one of approximating a system of ordinary differential equations, usually by some appropriate numerical time-stepping scheme. We will examine several methods that appeal to the second-order-in-time problem directly, as well as comment on those that work on a common reduction-of-order technique.

Begin by choosing a space $\mathcal{P}$ of polynomials and seek an approximate solution to (6) of the form

$$\boldsymbol{u}(\boldsymbol{x},t) \simeq p_n(\boldsymbol{x})\boldsymbol{\gamma}_n(t) = [p_n(\boldsymbol{x})\gamma_n^1(t), \ldots, p_n(\boldsymbol{x})\gamma_n^d(t)], x \in \Omega, t \geq 0.$$

Here again summation over repeated indices is assumed and superscript denotes the index of the time component. For example, if the displacement is

$$\boldsymbol{u}(\boldsymbol{x},t) = [u_1(\boldsymbol{x},t), \ldots, u_d(\boldsymbol{x},t)]^T$$

the first component is expanded as

$$u_1(\boldsymbol{x},t) = \sum_{n=1}^{\infty} p_n(\boldsymbol{x})\gamma_n^1(t).$$

For rectilinear domains, the functions $p_n(\boldsymbol{x})$ are generally taken to be products of one-dimensional polynomials as this gives a natural way to easily extend familiar families of orthogonal functions to higher dimensions. For more complex domains, affine mappings from tensor-product grids onto triangular meshes have been constructed and successfully implemented. For further discussion see (Warburton and Hestaven, 2008), (Canuto et al., 2007). For informal guidelines on choosing the space $\mathcal{P}$ depending on the types of boundary conditions that need to be satisfied as well as some discussion on rational orthogonal polynomials that satisfy radiation conditions a priori see (Boyd, 2001).

For our purposes we limit to the two dimensional case, and expand the displacements $\boldsymbol{u}(\boldsymbol{x},t) = (u(\boldsymbol{x},t), w(\boldsymbol{x},t))$, as well as the test functions $v(\boldsymbol{x})$ in a *nodal* approximation. That is, we let

$$u(\boldsymbol{x},t) = \sum_{i=1}^{N_p} u(t;\boldsymbol{x}_i)l_i(\boldsymbol{x}), w(\boldsymbol{x},t) = \sum_{i=1}^{N_p} w(t;\boldsymbol{x}_i)l_i(\boldsymbol{x}), v(\boldsymbol{x}) = \sum_{i=1}^{N_p} v(\boldsymbol{x}_i)l_i(\boldsymbol{x})$$

where

$$l_i(\boldsymbol{x}) = \prod_{j\neq i_1}^{N_p}\prod_{k\neq i_2}^{N_p} \frac{x-x_j}{x_{i_1}-x_j}\frac{y-y_k}{y_{i_2}-y_k}.$$

The functions $l_i(\boldsymbol{x})$, shown in Figures 1 and 2, act as discrete delta functions. That is, they have the property that

$$l_i(\boldsymbol{x}_j) = \begin{cases} 1, i = j \\ 0, i \neq j \end{cases}$$

In order to turn this into a numerical method, we then replace differentiation with multiplication by a pseudospectral differentiation matrix D, and integration by Gaussian quadrature. Construction of the differentiation matrix and quadrature formulas is addressed in the appendix, so for now we assure only that, for a given set of nodes, there exists a family of matrices that transform vectors of function values to their derivatives, and a vector of quadrature weights $\underline{\omega} = (\omega_k)$ that transforms integration into a dot-product.

For the two dimensional region Ω denote $\boldsymbol{x} = (x, z)$ and define D^x, D^z to be the differentiation matrices in the x, z directions respectively. We assume that Ω is a square region

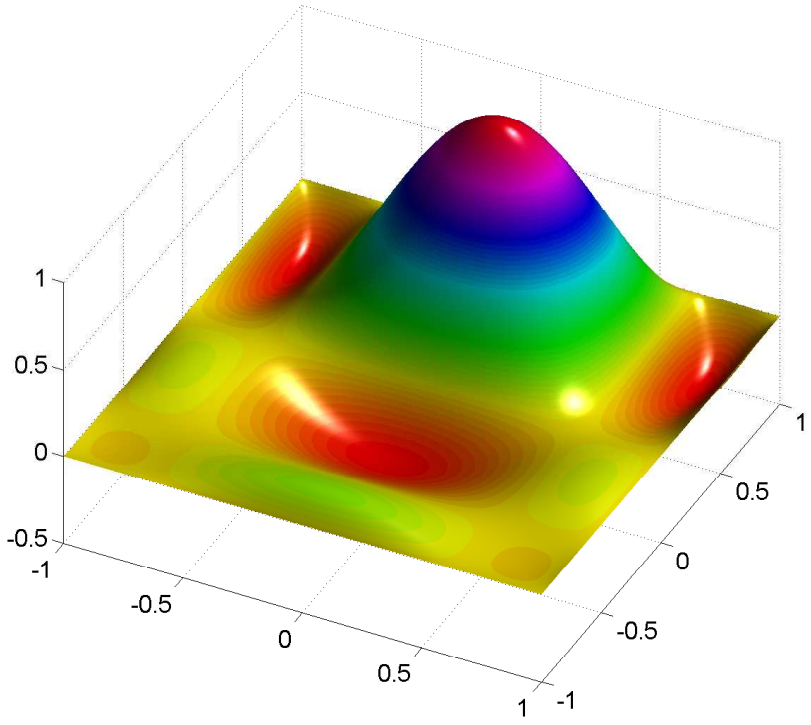

FIG. 1. A 2-dimensional Lagrange polynomial.

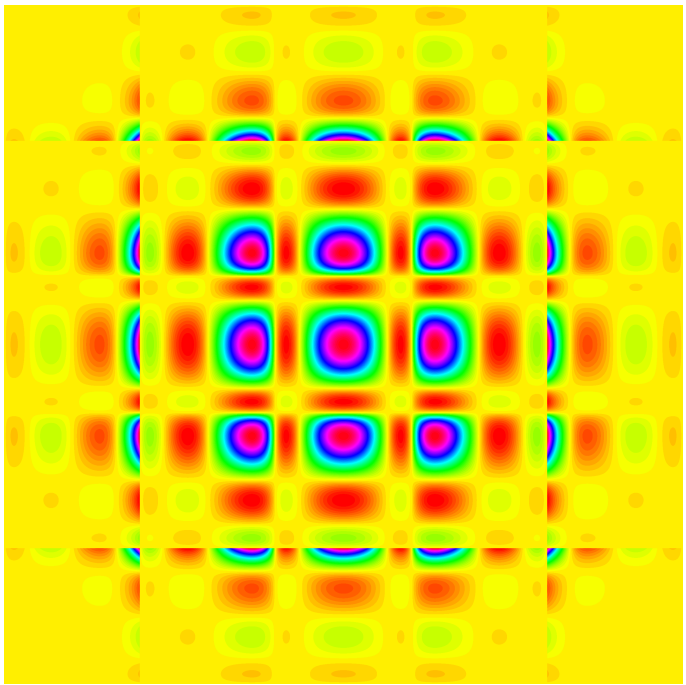

FIG. 2. A family of 25 2-dimensional Lagrange polynomials.

and its boundary is $\Gamma = \Gamma_N \cup \Gamma_S \cup \Gamma_E \cup \Gamma_w$ and we denote the quadrature weights associated with the inner-products on each of these boundary regions as $\underline{\omega}^N, \underline{\omega}^S, \underline{\omega}^E, \underline{\omega}^W$. The construction of the entire spatial discretization is tedious and so is omitted. One does notice when performing these calculations, however, that the inner-products in (6) reduce to 4 general cases which we address here by working directly with (3).

Let $\langle \cdot, \cdot \rangle$ be any of the inner-products in (3) and let ω be the associated quadrature weights. Then the inner-products in (3) all reduce to the following forms:

1.

$$\langle \rho \ddot{u}, v \rangle = \sum_{i=1}^{N_p} \sum_{j=1}^{N_p} \ddot{u}_i v_j \langle \rho l_i(\boldsymbol{x}), l_j(\boldsymbol{x}) \rangle = \sum_{i=1}^{N_p} \sum_{j=1}^{N_p} \sum_{k=1}^{N_p} \ddot{u}_i v_j \rho(\boldsymbol{x}_k) l_i(\boldsymbol{x}_k), l_j(\boldsymbol{x}_k) \omega_k$$

but $l_m(\boldsymbol{x}_n) = \delta_{mn}$ so this reduces to

$$\mathrm{diag}(\underline{v})\, \mathrm{diag}(\underline{\omega})\, \mathrm{diag}(\underline{\rho}) \underline{\ddot{u}}$$

where $\mathrm{diag}(\underline{v})$ is the matrix with the vector $\underline{v}$ along the main diagonal.

2.

$$\langle \lambda \partial_z w, \partial_x v \rangle = \sum_{i=1}^{N_p} \sum_{j=1}^{N_p} \sum_{k=1}^{N_p} w_i v_j \lambda(\boldsymbol{x}_k) \partial_z l_i(\boldsymbol{x}_k) \partial_x l_j(\boldsymbol{x}_k) \omega_k$$

However, $\partial_z l_i(\boldsymbol{x}_k) = D^z_{ki}$ and so we obtain

$$\mathrm{diag}(\underline{v})\, (D^x)^T\, \mathrm{diag}(\underline{\lambda})\, \mathrm{diag}(\omega) D^z \underline{u}.$$

3.

$$\langle f, v \rangle = \sum_{j=1}^{N_p} \sum_{k=1}^{N_p} v_j f(\boldsymbol{x}_k) l_j(\boldsymbol{x}_k) \omega_k = \mathrm{diag}(\underline{v})\, \mathrm{diag}(\underline{\omega}) \underline{f}.$$

4.

$$\langle \lambda \partial_x u \hat{n}, v \rangle = \sum_{i=1}^{N_p} \sum_{j=1}^{N_p} \sum_{k=1}^{N_p} u_i v_j \hat{n} \lambda(\boldsymbol{x}_k) \partial_x l_i(\boldsymbol{x}_k) l_j(\boldsymbol{x}_k) \omega_k$$

$$= \sum_{i=1}^{N_p} \sum_{k=1}^{N_p} u_i v_k \lambda(\boldsymbol{x}_k) \partial_x l_i(\boldsymbol{x}_k) \omega_k = \hat{n}\, \mathrm{diag}(\underline{v})\, \mathrm{diag}(\underline{\omega}) D^x \underline{u}.$$

The 4^{th} type corresponds to the boundary terms and is what allows us to *talk* to the boundary; incorporating absorbing and free-surface boundary conditions. The most appropriate absorbing boundary conditions for our purposes are those for which the time and space derivatives appear independently. We omit the details of the derivations here for the sake of brevity as even the two-dimensional case involves 16 boundary integrals, 8 of which account for the absorbing boundary conditions (all of which factor into a single operator). We note, however, that there are several different choices available and refer the reader

to (Stacey, 1988), (Sochacki, 1988) and (Quarteroni et al., 1998) for the construction and implementation of several higher-order methods that fit naturally into variational schemes.

Regardless of our treatment of boundary conditions we obtain, for the nodal values of the displacements in Ω at time $t > 0$, a second order system of ordinary differential equations

$$\begin{cases} M\ddot{\boldsymbol{U}}(t) + A\dot{\boldsymbol{U}}(t) + K\boldsymbol{U}(t) = \boldsymbol{F}(t) \\ \boldsymbol{U}(0) = \boldsymbol{U}_0 \\ \dot{\boldsymbol{U}}(0) = \boldsymbol{U}_1 \end{cases} \tag{7}$$

where $\boldsymbol{U}$ is a large vector of the nodal values of $u(\boldsymbol{x}, t)$ and $w(\boldsymbol{x}, t)$ and the matrices *M*, *A*, and *K* are all large, extremely sparse matrices. We may deal with this directly by using second-order-in-time centered-finite-differences for both the first and second derivatives. Replacing

$$\ddot{\boldsymbol{U}}(t_j) = \frac{\boldsymbol{U}(t_{j+1}) - 2\boldsymbol{U}(t_j) + \boldsymbol{U}(t_{j-1})}{dt^2} + O(t^2),\ \dot{\boldsymbol{U}}(t_j) = \frac{\boldsymbol{U}(t_{j+1}) - \boldsymbol{U}(t_{j-1})}{2dt} + O(t^2)$$

and dropping the error term, we obtain, for evolution in time

$$\left[M + \frac{dt}{2}A\right]\boldsymbol{U}(t_{j+1}) + \left[dt^2K - 2M\right]\boldsymbol{U}(t_j) + \left[M - \frac{dt}{2}A\right]\boldsymbol{U}(t_{j-1}) = dt^2\boldsymbol{F}(t_j).$$

For higher-order in time we can reduce (7) to a first order problem by making the substitution $\boldsymbol{V}(t) = \dot{\boldsymbol{U}}(t)$. This results in the problem

$$\begin{cases} \begin{pmatrix} I & 0 \\ 0 & M \end{pmatrix} \begin{pmatrix} \dot{\boldsymbol{U}} \\ \dot{\boldsymbol{V}} \end{pmatrix}(t) = \begin{pmatrix} 0 & I \\ K & A \end{pmatrix} \begin{pmatrix} \boldsymbol{U} \\ \boldsymbol{V} \end{pmatrix}(t) + \begin{pmatrix} 0 \\ \boldsymbol{F} \end{pmatrix}(t) \\ \begin{pmatrix} \boldsymbol{U} \\ \boldsymbol{V} \end{pmatrix}(0) = \begin{pmatrix} \boldsymbol{U}_0 \\ \boldsymbol{V}_0 \end{pmatrix} \end{cases} \tag{8}$$

This can be time-stepped by explicit higher-order, more computationally expensive, methods that have less prohibitive step-size requirements than explicit finite differences. Another possibility is to use the matrix exponential to compute the exact-in-time solution to (8), or to construct a fully-explicit time-stepping method with no step-size stability requirements. In general the matrices involved are huge and, for a large number of nodes, is not feasible computationally. However, if it were possible to construct such a matrix that was diagonalizable the computational cost would be reduced substantially. For a fixed problem, such a matrix could be stored to further reduce the computational cost.

NUMERICAL RESULTS

To test this we consider a forcing term with Ricker wavelet time-component

$$f(t) = \frac{2}{\sqrt{3\sigma}\pi^{\frac{1}{4}}}\left(1 - \frac{t^2}{\sigma^2}\right)e^{\frac{-t^2}{2\sigma^2}}$$

and conservative spatial component

$$(u_1(\mathbf{x}), w_1(\mathbf{x})) = -\nabla e^{-r\|\mathbf{x}-\mathbf{x_0}\|^2}$$

and propagate a 15 Hz wavelet in a 4500m square bipartite medium with properties listed in the following table.

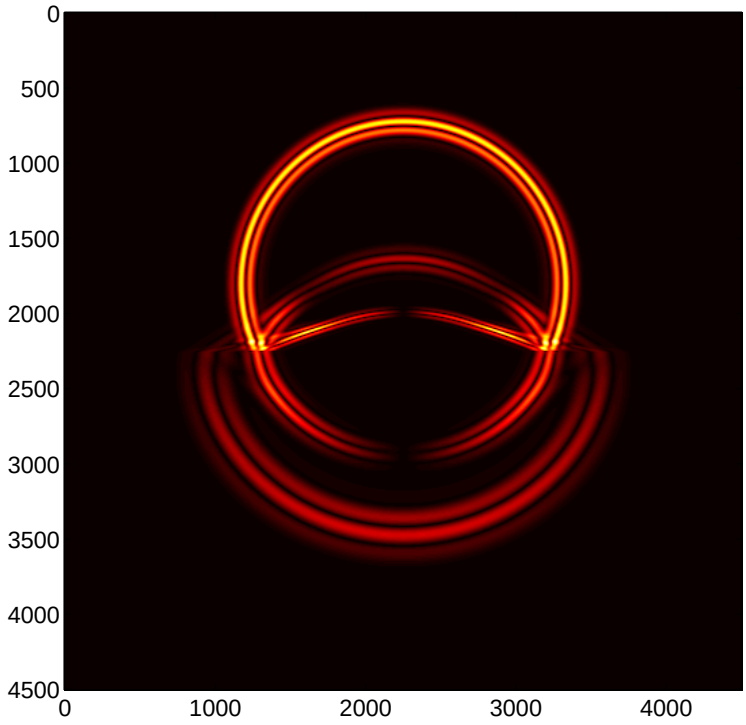

FIG. 3. Nodal Galerkin. Comp time = 206 s.

Region	ρ	V_p	V_s
1	2.064	2305	997
2	2.14	4500	2600

A nodal Galerkin method is compared to fourth and second order finite difference methods on a 501 by 501 node grid. Figures 3, 4 and 5 show the norm of the displacement for the three models propagated to 1 second and then normalized and clipped to exaggerate the dispersion effects. The extended arcs in the fourth-order model result from the wider stencil moving over the large step in the velocity model and then being propagated. Again, this is exaggerated here and is mainly due to the relatively small number of grid points we are using, but the effect is apparent.

The computation times are listed with the figures but are not very indicative of the associated computation costs of the three methods. The implementation of the three methods are nearly identical, with the only difference being the application of the derivative approximations. For the finite-difference methods the cost of this is $k * N^2$ where k is the width of the finite-difference stencil (3 for second order, 5 for fourth order). The differentiation matrices for the nodal Galerkin methods can be considered finite-difference matrices with stencils of width N and so the cost of applying these methods is N^3. We take $dt = .0008$ and so take 1179 steps to reach one second. We could take a smaller time step, but the one chosen assures us that the wavelet in time is well-represented and that the error associated with time stepping will not taint our results as we are more interested in spatial accuracy.

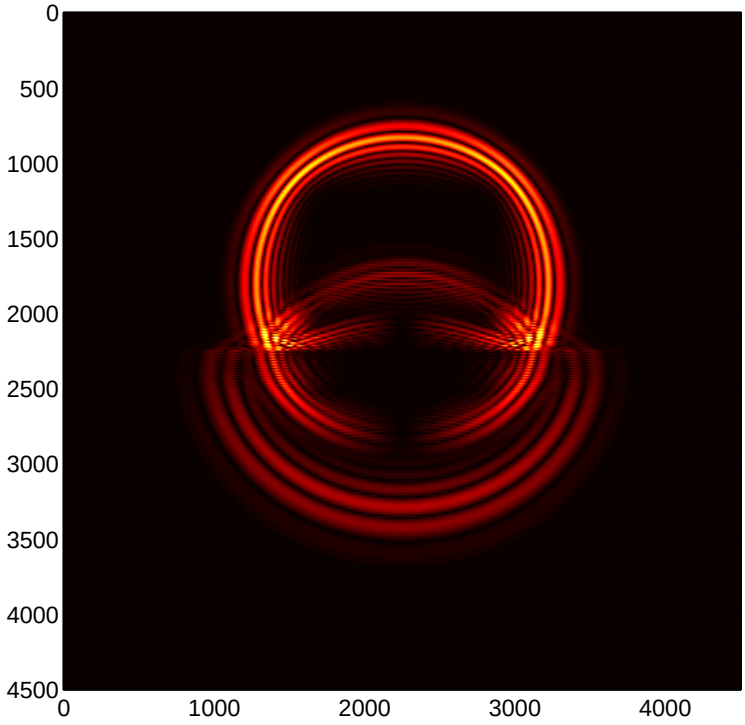

FIG. 4. Second-Order Finite Difference. Comp time = 64 s.

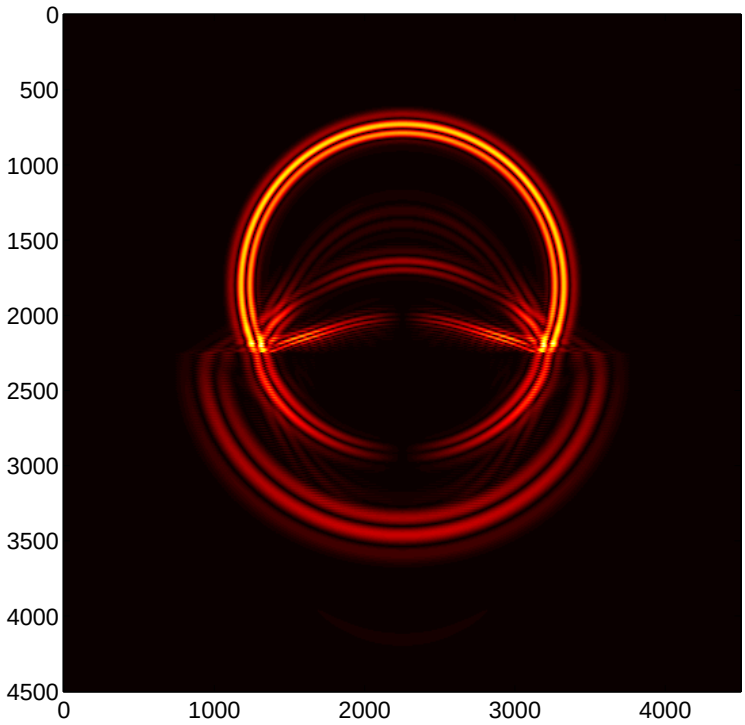

FIG. 5. Fourth-Order Finite Difference. Comp time = 75 s.

Locally the fourth order model approximates the wavefronts better than the second-order model (as is expected), but the size of the stencil means that we must alter it somehow at the boundaries, this is not the case with the differentiation matrices that appear in the nodal Galerkin methods as they are global and so for the approximation of the derivative at one node they take information from all other nodes in the model. In order to enforce different types of boundary conditions (such as clamped, Neumann, Dirichlet, periodic, etc...) the first and last rows and columns of the differentiation matrix must be altered.

Figures 6 and 7 show comparisons of the centerline of the model ($x = 2250$, for all z) at time corresponding wavefront in various regions of the velocity model. The amplitude error associated with the second-order stencil is apparent as is the dispersion of all three methods near a jump. Figure 8 shows a close-up of the region of the model at the jump

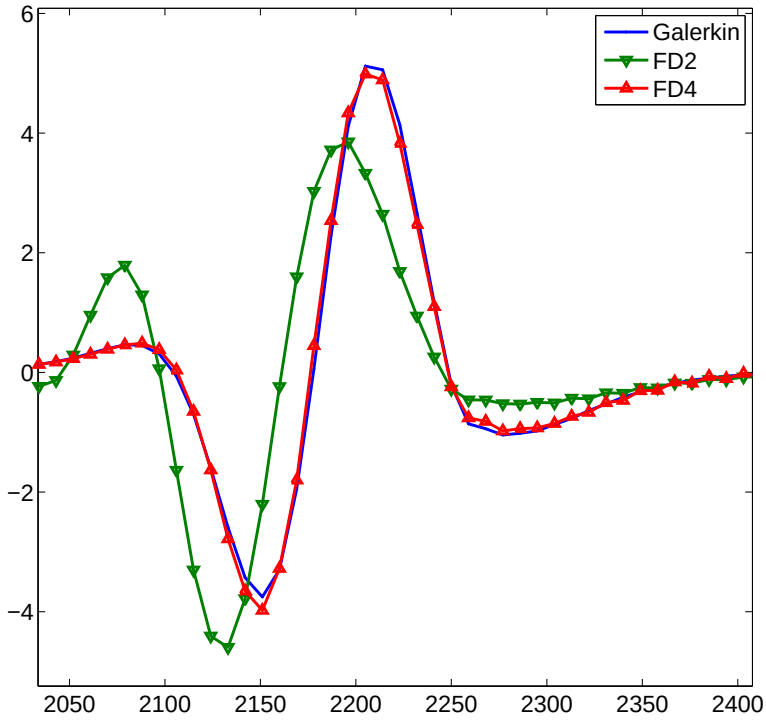

FIG. 6. Close-up of the centerline of the horizontal component of a 2D elastic wave propagated to $t = .4150$ sec. The region plotted shows the disagreement of the three methods in a smooth region of the velocity model.

at $t = 1$ second where the incident P-wave is being trasmitted and reflected. The RGB colour channels in the image correspond to the directions of the displacement as listed in the following table.cement as listed in the following table.

Displacement	Positive	Negative
Horizontal	R	R + G
Vertical	B	B + G

Figures 9, 10 and 11 show the vector field of the same region at varying levels of zoom.

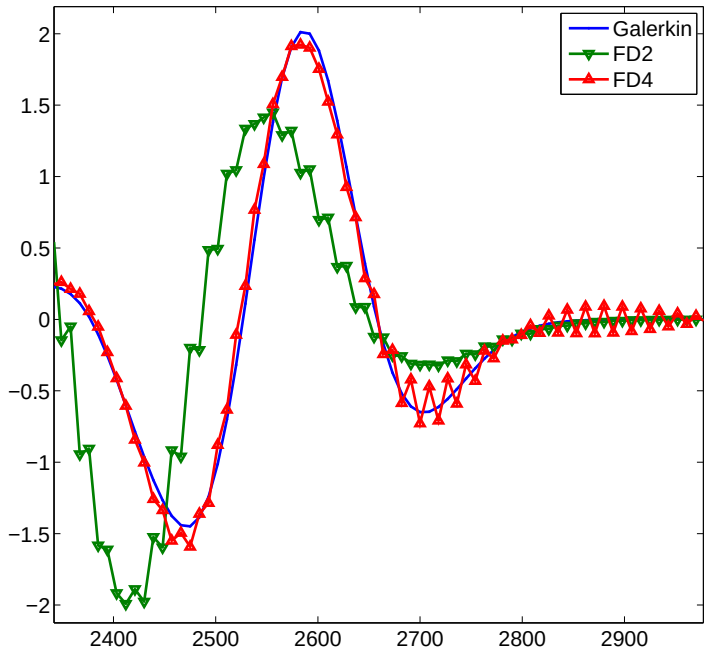

FIG. 7. Close-up of the centerline of the horizontal component of a 2D elastic wave propagated to $t = .6$ sec. The region plotted shows the disagreement of the three methods in a the presence of a sharp jump in the velocity model.

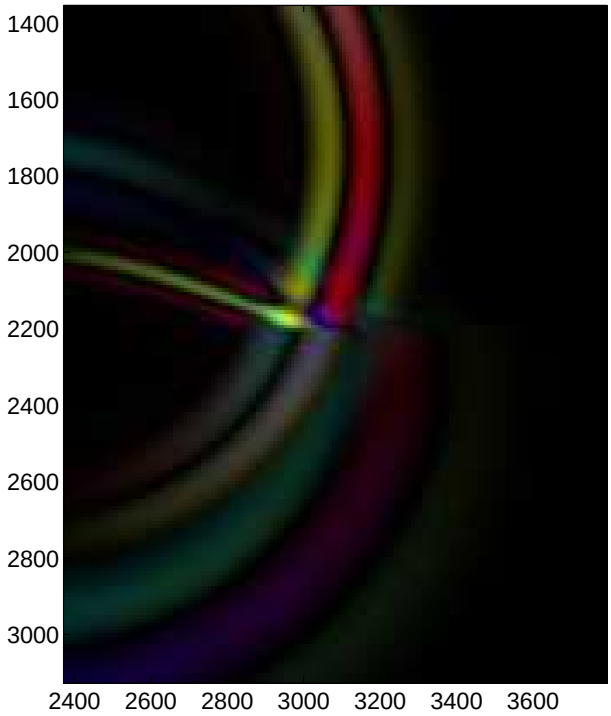

FIG. 8. A P-wave being converted into reflected and transmitted P and S waves

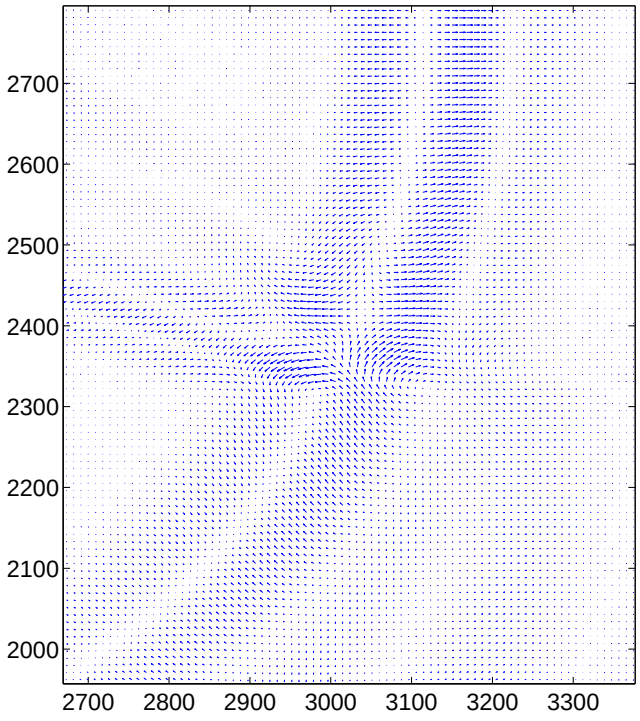

FIG. 9. Vector field of a P-wave being converted into reflected and transmitted P and S waves

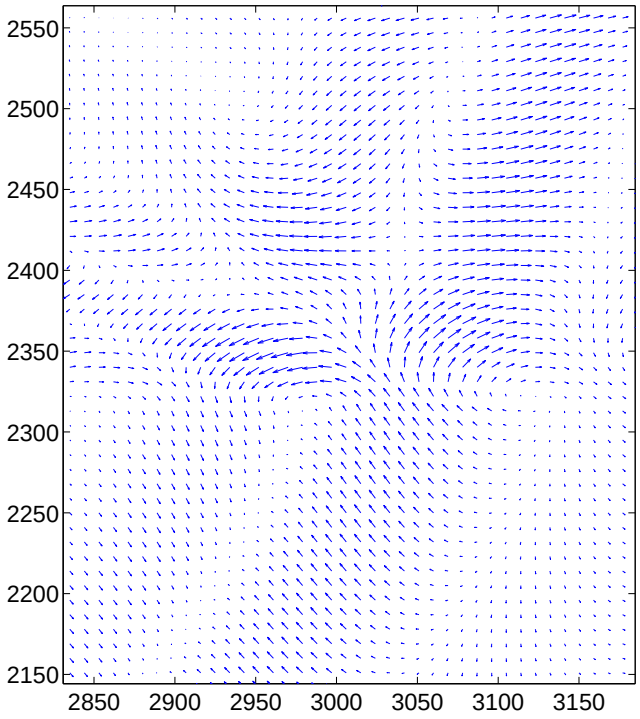

FIG. 10. Vector field of a P-wave being converted into reflected and transmitted P and S waves

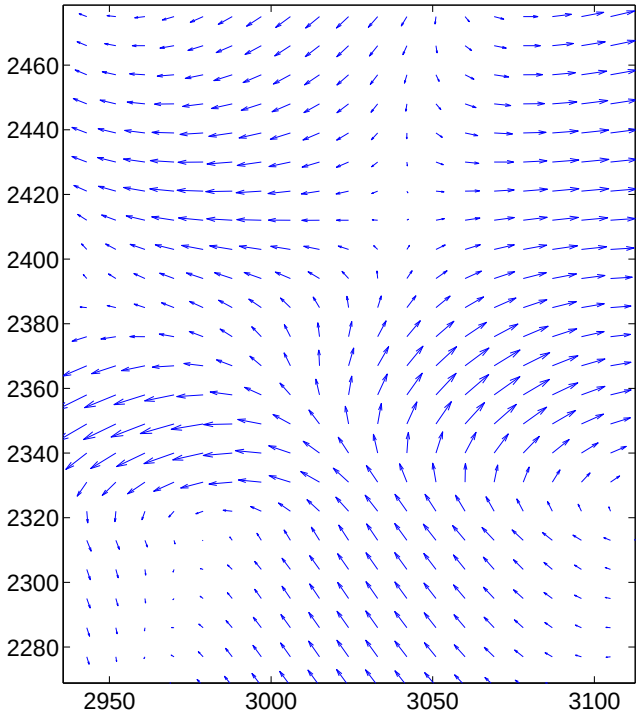

FIG. 11. Vector field of a P-wave being converted into reflected and transmitted P and S waves

To test the absorbing boundary conditions we initiate a P-wave in a homogeneous media with $Vp = 4500$, $Vs = 2600$ and $\rho = 2.14$. We then allow the wave to propagate to time $t = 1$ and place absorbing boundaries on the horizontal edges. Figure 12 shows the reflection of the displacement. As is expected, the magnitude of the reflected wave is nearly zero as the p-wave hits the boundary head-on and increases as the angle of incidence reaches $90°$.

APPENDIX

In order to be as general as possible, assume a function f can be expanded in such a way that the series coefficients, a_n, are chosen so approximation interpolates f on a set of grid points $\{\xi_i | i = 1, \ldots, N_p\}$. This is possible since it strictly yields a set of N_p equations for the N_p unknowns $\{a_n\}_{n=1}^{N_p}$. The points used may be arbitrary but are generally chosen to be a set of Gauss-Lobatto points whose quadrature weight-function $w(x)$ is most suitable to the problem at hand. These are the zeros of the N_p^{th} order Jacobi polynomial, defined as the (α, β)-family of solutions to the singular Sturm-Liouville eigenvalue problem

$$\frac{d}{dx}(1-x^2)w(x)\frac{d}{dx}P_n^{(\alpha,\beta)}(x) + n(n+\alpha+\beta+1)w(x)P_n^{(\alpha,\beta)}(x) = 0, x \in [-1,1],$$

$$w(x) = (1-x)^\alpha(1+x)^\beta.$$

For general purposes this is usually the Legendre-Gauss-Lobatto (LGL) points, chosen by $\alpha = 0, \beta = 0$, yielding the Legendre polynomials with weight function $w(x) = 1$. There

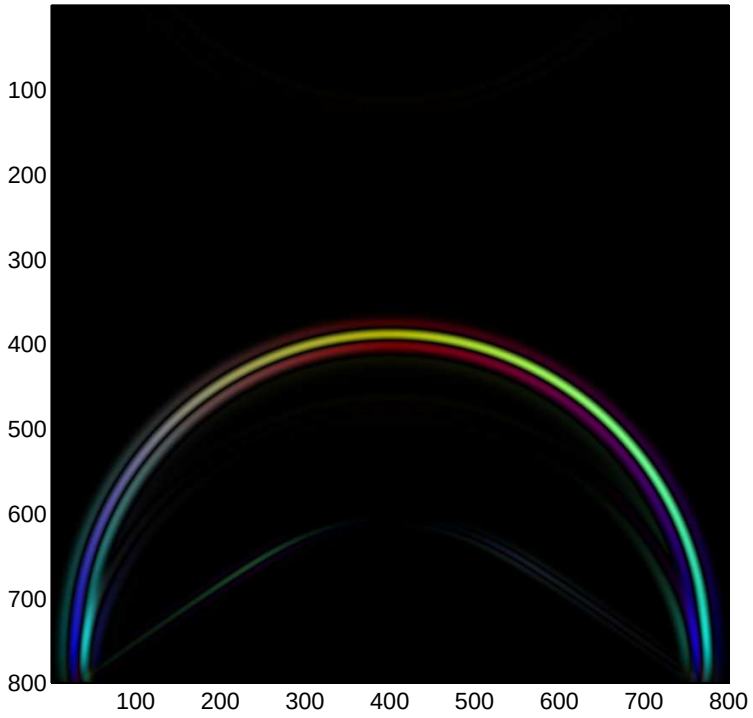

FIG. 12. Boundary reflections from incident P-wave

is no closed form expression for the LGL points, and so they are computed numerically by a suitable root-finding method. This can be done at the same time as one computes the Legendre polynomials using standard recursion methods.

Once a set of points is chosen we have two equal approximations

$$f(x) \simeq \sum_{n=1}^{N_p} a_n \varphi_n(x) = \sum_{i=1}^{N_p} f(\xi_i) l_i(x) \tag{9}$$

where the $l_i(x)$ are the Lagrange interpolating polynomials defined as

$$l_i(x) = \prod_{j \neq i}^{N_p} \frac{x - \xi_j}{\xi_i - \xi_j}.$$

We may then write

$$\underbrace{\begin{pmatrix} f(\xi_1) \\ f(\xi_2) \\ \vdots \\ f(\xi_n) \end{pmatrix}}_{\underline{\tilde{f}}} = \underbrace{\begin{pmatrix} \varphi_1(\xi_1) \dots \varphi_n(\xi_1) \\ \varphi_1(\xi_2) \dots \varphi_n(\xi_2) \\ \dots \quad \dots \quad \dots \\ \varphi_1(\xi_n) \dots \varphi_n(\xi_n) \end{pmatrix}}_{\Phi} \underbrace{\begin{pmatrix} a_1 \\ a_2 \\ \vdots \\ a_n \end{pmatrix}}_{\tilde{a}} \tag{10}$$

and the interpolary approximation

$$\underbrace{\begin{pmatrix} \varphi_1(x) \\ \varphi_2(x) \\ \vdots \\ \varphi_n(x) \end{pmatrix}}_{\tilde{\varphi}} = \underbrace{\begin{pmatrix} \varphi_1(\xi_1) \dots \varphi_1(\xi_n) \\ \varphi_2(\xi_1) \dots \varphi_2(\xi_n) \\ \dots \quad \dots \quad \dots \\ \varphi_n(\xi_1) \dots \varphi_n(\xi_n) \end{pmatrix}}_{\Phi^T} \underbrace{\begin{pmatrix} l_1(x) \\ l_2(x) \\ \vdots \\ l_n(x) \end{pmatrix}}_{\tilde{l}}.$$

Differentiating (7) yields

$$f'(x) = \sum_{i=1}^{N_p} f(\xi_i) l_i'(x)$$

or

$$\underbrace{\begin{pmatrix} f'(\xi_1) \\ f'(\xi_2) \\ \vdots \\ f'(\xi_n) \end{pmatrix}}_{\tilde{f}'} = \underbrace{\begin{pmatrix} l_1'(\xi_1) \dots l_n'(\xi_1) \\ l_1'(\xi_2) \dots l_n'(\xi_2) \\ \dots \quad \dots \quad \dots \\ l_1'(\xi_n) \dots l_n'(\xi_n) \end{pmatrix}}_{D_x} \underbrace{\begin{pmatrix} f(\xi_1) \\ f(\xi_2) \\ \vdots \\ f(\xi_n) \end{pmatrix}}_{\tilde{f}}.$$

and using (8) we have the relationship

$$\underbrace{\begin{pmatrix} \varphi_1'(\xi_1) \dots \varphi_1'(\xi_n) \\ \varphi_2'(\xi_1) \dots \varphi_2'(\xi_n) \\ \dots \quad \dots \quad \dots \\ \varphi_n'(\xi_1) \dots \varphi_n'(\xi_n) \end{pmatrix}}_{\Phi_x^T} = \underbrace{\begin{pmatrix} \varphi_1(\xi_1) \dots \varphi_1(\xi_n) \\ \varphi_2(\xi_1) \dots \varphi_2(\xi_n) \\ \dots \quad \dots \quad \dots \\ \varphi_n(\xi_1) \dots \varphi_n(\xi_n) \end{pmatrix}}_{\Phi^T} \underbrace{\begin{pmatrix} l_1'(\xi_1) \dots l_1'(\xi_n) \\ l_2'(\xi_1) \dots l_2'(\xi_n) \\ \dots \quad \dots \quad \dots \\ l_n'(\xi_1) \dots l_n'(\xi_n) \end{pmatrix}}_{D^T}$$

and so the matrix D, which maps a vector of function values to derivative values can be computed directly as $D = \Phi_x \Phi^{-1}$ for any set of arbitrary points as long as one can invert the matrix Φ. In practice this is not always possible. For example, when using the Legendre polynomials, Φ is a Vandermonde matrix and is ill-conditioned at the set of equidistant points. Choosing the LGL points however, fixes this problem. An in-depth analysis of these problems is found in (Warburton, 2008).

In two-dimensions, a region Ω is mapped onto the reference square $[-1,1]^2$. As most models are defined on $[0, x_{\max}] \times [0, z_{\max}]$ this is achieved by the affine mapping

$$F : [0, x_{\max}] \times [0, z_{\max}] \to [-1,1]^2 : (x,z) \mapsto \left(\frac{2x}{x_{\max}} - 1, \frac{2z}{z_{\max}} - 1 \right)$$

with inverse

$$F^{-1} : [-1,1]^2 \to [0, x_{\max}] \times [0, z_{\max}] : (\xi, \eta) \mapsto \left(x_{\max} \frac{\xi + 1}{2}, z_{\max} \frac{\eta + 1}{2} \right)$$

The Jacobian of the map is constant so its implementation is achieved by performing all calculations on $[-1,1]^2$ and multiplying the associated quadrature weights by the Jacobian of the mapping.

ACKNOWLEDGMENTS

We gratefully acknowledge the continued support of MITACS through the POTSI research project and its industrial collaborators, the support of NSERC through the CREWES consortium and its industrial sponsors, and support of the Pacific Institute for the Mathematical Sciences.

REFERENCES

Atkinson, K. E., and Han, W., 2009, Theoretical Numerical Analysis: A Functional Analysis Framework: Springer.

Boyd, J. P., 2001, Chebyshev and Fourier spectral methods Second edition: Dover.

Canuto, C., Hussaini, M. Y., Quarteroni, A., and Zang., T. A., 2007, Spectral Methods: Evolution to Complex Geometries and Applications to Fluid Dynamics: Springer.

Horgan, C. O., 1995, Korn's inequalities and their applications in continuum mechanics: SIAM Rev., **37**, 491–511.

Quarteroni, A., Tagliani, A., and Zampieri, E., 1998, Generalized galerkin approximations of elastic waves with absorbing boundary conditions: Computer Methods in Applied Mechanics and Engineering, **163**, No. 1-4, 323 – 341.

Sochacki, J., 1988, Absorbing boundary conditions for the elastic wave equations: Applied Mathematics and Computation, **28**, No. 1, 1 – 14.

Stacey, R. ., 1988, Improved transparent boundary formations for the elastic-wave equation: Bulletin of the Seismological Society of America, **78**, 2089–2097.

Warburton, T., and Hestaven, J. S., 2008, Nodal Discontinuous Galerkin Methods: Algorithms, Analysis and Applications: Springer.

Zienkiewicz, O. C., Taylor, R. L., and Zhu, J. Z., 2005, The Finite Element Method: Its Basis and Fundamentals: Elsevier.